AIRS/AMSU/HSB Precipitation Estimates

Frederick W. Chen, *Student Member, IEEE,* and David H. Staelin, *Fellow, IEEE*

***Abstract*—Precipitation rates (millimeters per hour) with 15- and 50-km horizontal resolution are among the initial products of Atmospheric Infrared Sounder/Advanced Microwave Sounding Unit/Humidity Sounder for Brazil (AIRS/AMSU/HSB). They will help identify the meteorological state of the atmosphere and any AIRS soundings potentially contaminated by precipitation. These retrieval methods can also be applied to the AMSU 23–191-GHz data from operational weather satellites such as NOAA-15, -16, and -17. The global extension and calibration of these methods are subjects for future research. The precipitation-rate estimation method presented is based on the opaque-channel approach described by Staelin and Chen, but it utilizes more channels (17) and training data and infers 54-GHz band radiance perturbations at 15-km resolution. The dynamic range now reaches 100 mm/h. The method utilizes neural networks trained using the National Weather Service's Next Generation Weather Radar (NEXRAD) precipitation estimates for 38 coincident rainy orbits of NOAA-15 AMSU data obtained over the eastern United States and coastal waters during a full year. The rms discrepancies between AMSU and NEXRAD were evaluated for the following NEXRAD rain-rate categories: $<$0.5, 0.5–1, 1–2, 2–4, 4–8, 8–16, 16–32, and $>$32 mm/h. The rms discrepancies for the 3790 15-km pixels not used to train the estimator were 1.0, 2.0, 2.3, 2.7, 3.5, 6.9, 19.0, and 42.9 mm/h, respectively. The 50-km retrievals were computed by spatially filtering the 15-km retrievals. The rms discrepancies over the same categories for all 4709 50-km pixels flagged as potentially precipitating were 0.5, 0.9, 1.1, 1.8, 3.2, 6.6, 12.9, and 22.1 mm/h, respectively. Representative images of precipitation for tropical, mid-latitude, and snow conditions suggest the method's potential global applicability.**

***Index Terms*—Hydrology, measurement, microwave propagation, microwave radiometry, precipitation, rain rate, remote sensing, weather satellite.**

I. Introduction

GLOBAL precipitation observations are important for both scientific and operational purposes. It is also important to identify Aqua Atmospheric Infrared Sounder (AIRS) atmospheric soundings that might be contaminated by precipitation. The present paper introduces improvements to the precipitation detection and retrieval technique of Staelin and Chen [1], which utilized the Advanced Microwave Sounding Unit (AMSU) on the United States NOAA-15 satellite. This neural-network-based technique retrieves precipitation rates by using opaque oxygen and water vapor channels near 54 and 183 GHz, respectively, that are indirectly responsive to vertical wind velocity and humidity; precipitation rate is approximately proportional to the product of vertical wind and absolute humidity. The vertical wind is correlated with cell-top altitude, microwave albedo, and hydrometeor diameters, all of which influence the microwave spectrum 50–200 GHz independently. These opaque-channel methods differ from the traditional window-channel methods that rely upon visible contrast between the surface and precipitation [2]–[5].

TABLE I
AQUA AMSU/HSB CHANNEL FREQUENCIES

AMSU Channels		
Channel	Center Frequencies (MHz)	Bandwidth (MHz)
1	23,800 ± 72.5	2x125
2	31,400 ± 50	2x80
3	50,300 ± 50	2x80
4	52,800 ± 105	2x190
5	53,596 ± 115	2x168
6	54,400 ± 105	2x190
7	54,940 ± 105	2x190
8	55,500 ± 87.5	2x155
9	57,290.344 = f_{LO} ± 87.5	2x155
10	f_{LO} ± 217	2x77
11	f_{LO} ± 322.2 ± 48	4x35
12	f_{LO} ± 322.2 ± 22	4x15
13	f_{LO} ± 322.2 ± 10	4x8
14	f_{LO} ± 322.2 ± 4.5	4x3
15	89,000 ± 900	2x1000
HSB Channels		
Channel	Center Frequencies (GHz)	Bandwidth (GHz)
1	150 ± 0.9	2x1
2	183.31 ± 1	2x0.5
3	183.31 ± 3	2x1
4	183.31 ± 7	2x2

On Aqua, the Humidity Sounder for Brazil (HSB) replaced the 15-km-resolution 89–191-GHz module (AMSU-B) used on NOAA-15; the 50-km-resolution 23.6–91-GHz module (AMSU-A) remains and is referred to as AMSU. AMSU/HSB on Aqua nearly duplicates AMSU on NOAA-15, except that the 15-km-resolution 89-GHz channel has been omitted. This channel was not used in the retrievals analyzed in this paper. Table I characterizes the AMSU/HSB microwave channels, and a more complete description of AMSU/HSB is presented in this issue by Lambrigtsen [2]. The notation in the table indicates that Channel 1 of AMSU, for example, has 125-MHz sidebands centered at 23 800±72.5 GHz.

The current Aqua precipitation retrieval algorithms are superior to those presented previously [1] in that the following occur.

1) NOAA-15 training data were less perturbed by radio frequency interference starting October 1999, permitting the 183 ± 3-GHz and other HSB bands to be used satisfactorily without correction.
2) Seasonally balanced training dataset was used.

Manuscript received March 19, 2002; revised November 15, 2002. This work was supported by the National Aeronautics and Space Administration under Grant NAG5-7487 and Contract NAS5-31376.

The authors are with the Research Laboratory of Electronics, Massachusetts Institute of Technology, Cambridge, MA 02139 USA (e-mail: staelin@mit.edu).

Digital Object Identifier 10.1109/TGRS.2002.808322

3) Passive microwave temperature and water vapor profile information was added.
4) Fifteen-kilometer perturbations of the 50-km 54-GHz band AMSU channels are inferred by combining the spatial information in the 15-km 183-GHz channels with the radiance information in the 50-km channels.
5) More reliable winter retrievals were obtained by using 183 ± 3-GHz data.
6) Algorithm was trained using National Weather Service's Next Generation Weather Radar (NEXRAD) data only at ranges 30–110 km from each radar.

Experimental validation of precipitation sensors typically involves comparisons with rain gauges, radar, and other sensors, each of which has its own characteristics and limitations. Several methods are to be tested with the Aqua mission and its co-orbiting satellites. For example, CloudSat [3] will carry a 94-GHz precipitation imaging radar. Relevant instruments on Aqua include the Advanced Microwave Scanning Radiometer-EOS (AMSR-E), the Moderate Resolution Imaging Spectroradiometer (MODIS), and AIRS itself. All will view precipitation observed by NEXRAD, rain gauges, and other sensors nearly simultaneously. This inter-instrument data fusion and cross-validation effort will be a major activity of Aqua.

Prior studies of passive microwave window-channel methods have discussed the substantial challenge of validating precipitation retrievals (e.g., PIP-1, PIP-2, PIP-3, AIP-1, AIP-2, and AIP-3) [4]–[6]. The challenges posed by sporadic behavior and imperfect data overlap are compounded by weaknesses in rain gauge data (e.g., wind effects) and radar data (e.g., undetected anomalous propagation). Ultimately, as AMSU/HSB validation efforts expand to include multiple noncoincident sensor types, similar averaging and statistical analysis methods will be required. An early objective of such comparisons will be to correct for any systematic training biases introduced by the 3-GHz radar data which depend on the assumed Z–R relationship and generally respond more strongly to hail and the bright band and less strongly to drizzle and dry snowfall. Combining such passive and active microwave precipitation data with better physics-based models should permit still further improvement.

The following sections of this paper present the precipitation-rate retrieval algorithm (Section II), quantitative comparisons of AIRS/AMSU/HSB and NEXRAD retrievals (Section III), regional and global examples of retrievals that illustrate the range of climates for which these retrievals are meteorologically relevant, including snowfall (Section IV), and conclusions (Section V).

II. Precipitation Retrieval Algorithms

A. Overview

The current AMSU/HSB precipitation retrieval algorithm is based on NOAA-15 AMSU comparisons with NEXRAD over the eastern United States during 38 orbits that exhibited significant precipitation and were distributed throughout the year. These orbits are listed in Table II. The primary precipitation-rate retrieval products of AMSU/HSB are ~15- and ~50-km-resolution contiguous retrievals over the viewing positions of HSB and AMSU, respectively, within 43° of nadir. The two outermost 50-km and six outermost 15-km viewing positions on each side of the swath are omitted due to their grazing angles. After the algorithm architectures for these two retrieval methods are presented below, the derivation of the numerical coefficients characterizing the neural network is described.

TABLE II
List of Rainy Orbits Used for Training, Validation, and Testing

16 Oct 1999, 0030 UTC	30 Apr 2000, 1430 UTC
31 Oct 1999, 0130 UTC	14 May 2000, 0030 UTC
2 Nov 1999, 0045 UTC	19 May 2000, 0015 UTC
4 Dec 1999, 1445 UTC	19 May 2000, 0145 UTC
12 Dec 1999, 0100 UTC	20 May 2000, 0130 UTC
28 Jan 2000, 0200 UTC	25 May 2000, 0115 UTC
31 Jan 2000, 0045 UTC	10 Jun 2000, 0200 UTC
14 Feb 2000, 0045 UTC	16 Jun 2000, 0130 UTC
27 Feb 2000, 0045 UTC	30 Jun 2000, 0115 UTC
11 Mar 2000, 0100 UTC	4 Jul 2000, 0115 UTC
17 Mar 2000, 0015 UTC	15 Jul 2000, 0030 UTC
17 Mar 2000, 0200 UTC	1 Aug 2000, 0045 UTC
19 Mar 2000, 0115 UTC	8 Aug 2000, 0145 UTC
2 Apr 2000, 0100 UTC	18 Aug 2000, 0115 UTC
4 Apr 2000, 0015 UTC	23 Aug 2000, 1315 UTC
8 Apr 2000, 0030 UTC	23 Sep 2000, 1315 UTC
12 Apr 2000, 0045 UTC	5 Oct 2000, 0130 UTC
12 Apr 2000, 0215 UTC	6 Oct 2000, 0100 UTC
20 Apr 2000, 0100 UTC	14 Oct 2000, 0130 UTC

B. Fifteen- and 50-km Retrieval Algorithms

The 15-km-resolution precipitation-rate retrieval algorithm, summarized in Figs. 1 and 2, begins with identification of potentially precipitating pixels. All 15-km pixels with brightness temperatures at 183 ± 7 GHz that are below a threshold T_7 are flagged as potentially precipitating, where

$$T_7 = 0.667(T_{53.6} - 248) + 252 + 6\cos\theta \tag{1}$$

and where θ is the satellite zenith angle and $T_{53.6}$ is the spatially filtered 53.6-GHz brightness temperature obtained by selecting the warmest brightness temperature within a 7×7 array of AMSU-B pixels. If, however, $T_{53.6}$ is below 248 K, then the brightness temperature at 183 ± 3 GHz is compared instead to a different threshold T_3, where

$$T_3 = 242.5 + 5\cos\theta. \tag{2}$$

The 183 ± 3-GHz band is used to flag potential precipitation when the 183 ± 7-GHz flag could be erroneously set by low surface emissivity in very cold dry atmospheres, as indicated by $T_{53.6}$. These thresholds T_7 and T_3 are slightly colder than a saturated atmosphere would be, implying the presence of a microwave-absorbing cloud. If the locally filtered $T_{53.6}$ is less than 242 K, then the pixel is assumed not to be precipitating.

Within these flagged regions, strong precipitation is generally characterized by cold cloud-induced perturbations of the AMSU-A tropospheric temperature sounding channels in the range 52.5–55.6 GHz. Examples of 183 ± 7-GHz data and the corresponding 50-km cold perturbations at 52.8 GHz are illustrated in Fig. 3(a) and (c). Physical considerations and aircraft data show that convective cells near 54 GHz typically appear slightly off-center and less extended relative to the 183-GHz

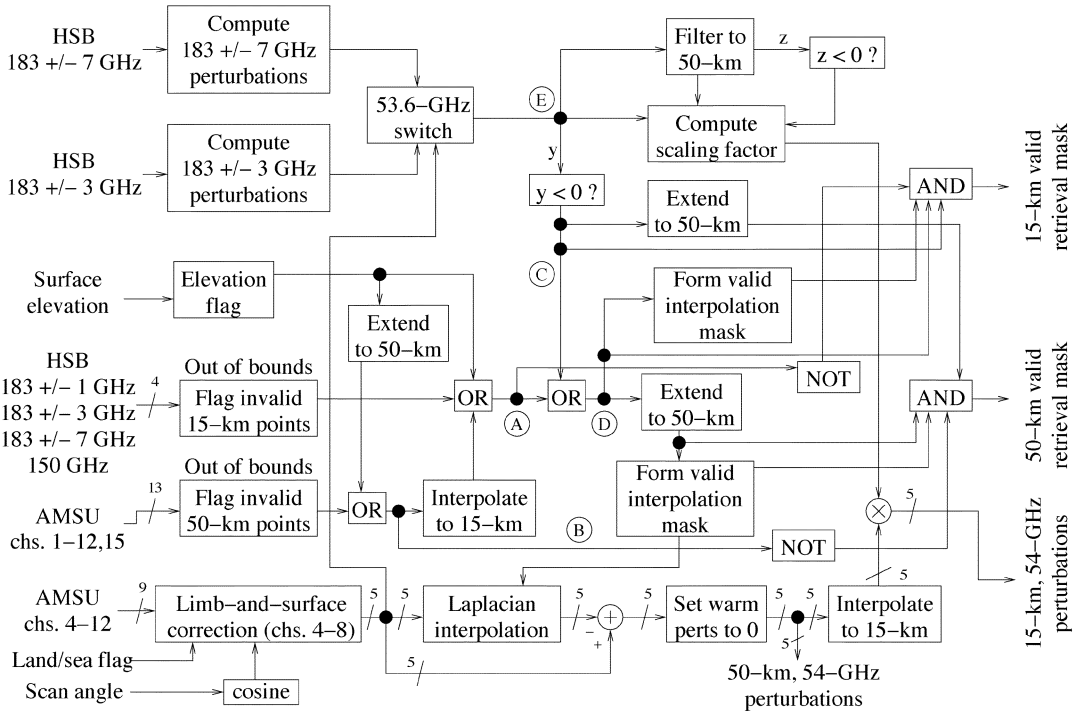

Fig. 1. Precipitation-rate retrieval algorithm, first stage.

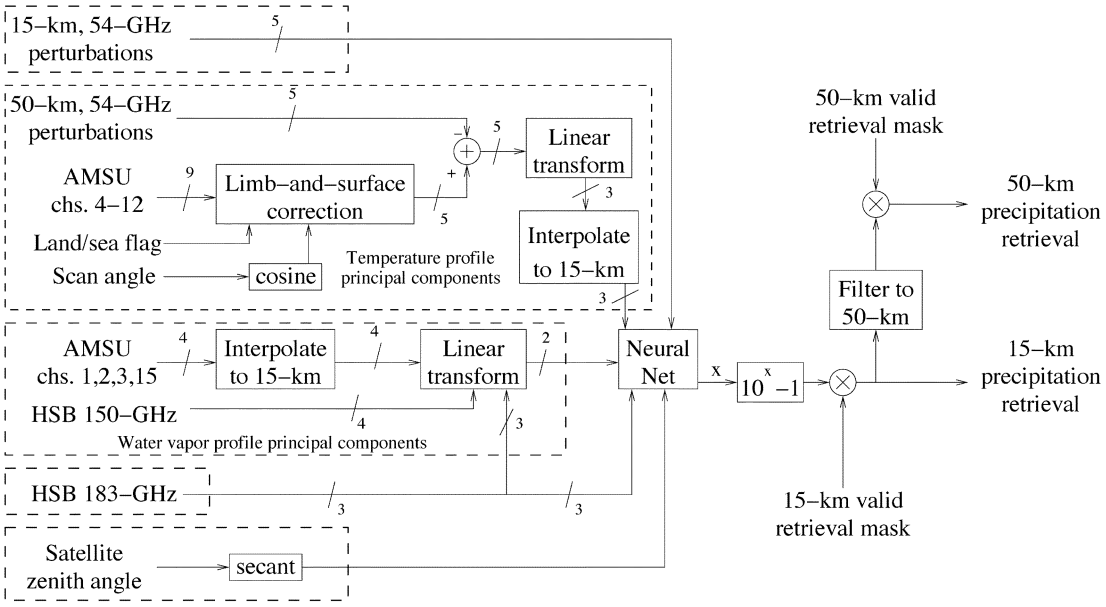

Fig. 2. Precipitation-rate retrieval algorithm, final stage.

images [7], [8]. The small interpolation errors in converting 54-GHz perturbations to 15-km contribute to the total errors and discrepancies discussed in Section III. These 50-km-resolution 52.8-GHz perturbations $\Delta T_{50,\,52.8}$ are then used to infer the perturbations $\Delta T_{15,\,52.8}$ [see Fig. 3(d)] that might have been observed at 52.8 GHz with 15-km resolution had those perturbations been distributed spatially in the same way as the cold perturbations observed at either 183±7 or 183±3 GHz, the choice between these two channels being the same as described above. This requires the bilinearly interpolated 50-km AMSU data to be resampled at the HSB beam positions. These inferred 15-km perturbations are computed for five AMSU-A channels using

$$\Delta T_{15,\,54} = (\Delta T_{15,\,183}/\Delta T_{50,\,183})\Delta T_{50,\,54}. \tag{3}$$

The perturbation $\Delta T_{15,\,183}$ near 183 GHz is defined to be the difference between the observed radiance and the appropriate threshold given by (1) or (2). The perturbation $\Delta T_{50,\,54}$ near 54 GHz is defined to be the difference between the observed radiance and the Laplacian-interpolated radiance based

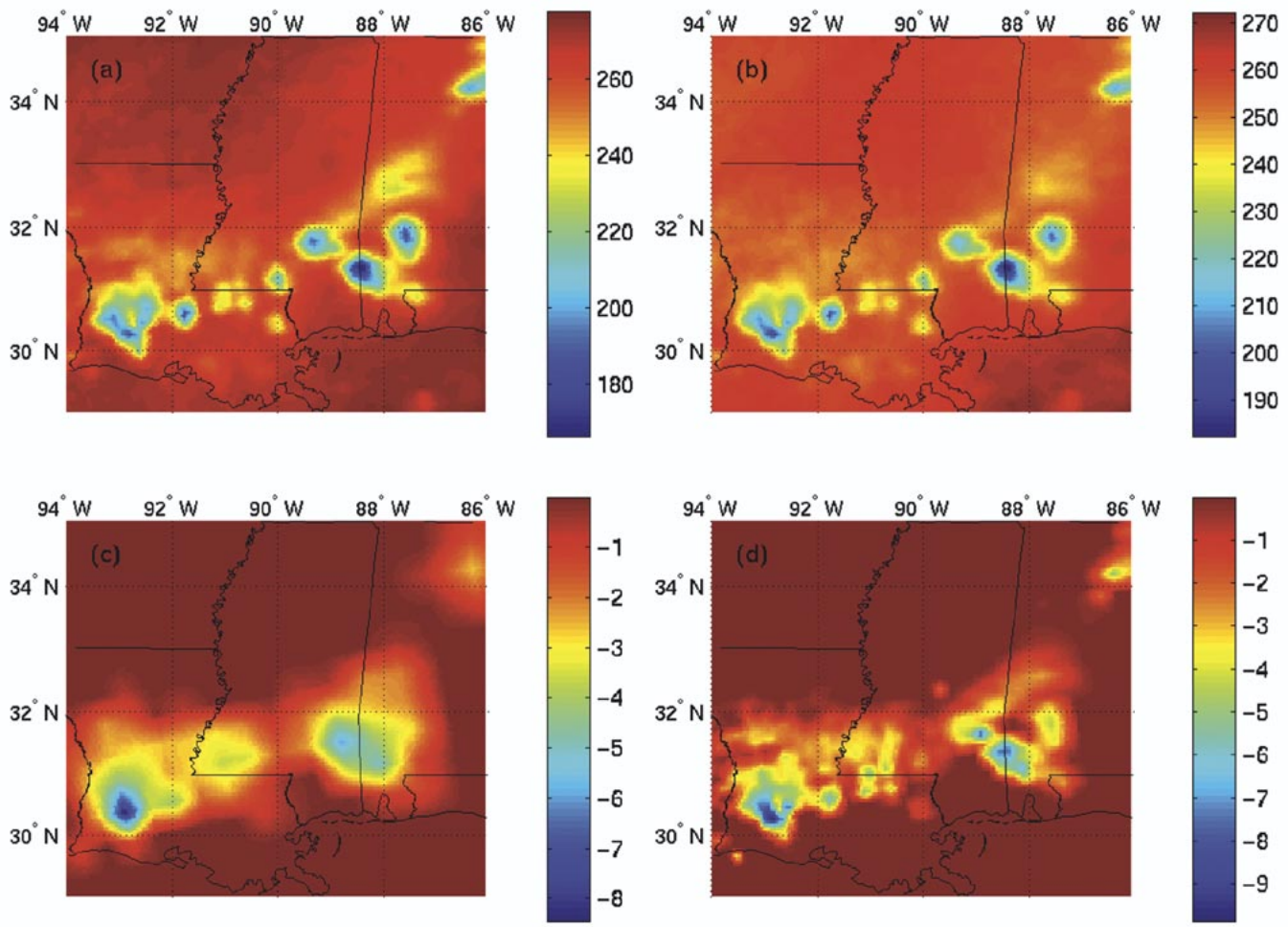

Fig. 3. Frontal system September 13, 2000, 0130 UTC. (a) Brightness temperatures near 183±7 GHz. (b) Brightness temperatures near 183±3 GHz. (c) Brightness temperature perturbations near 52.8 GHz. (d) Inferred 15-km-resolution brightness temperature perturbations near 52.8 GHz.

on those pixels surrounding the flagged region [1]. Any warm perturbations in the images of $\Delta T_{15,183}$ and $\Delta T_{50,54}$ are set to zero. Limb- and surface-emissivity corrections to nadir for the five 54-GHz channels are produced by neural networks for each channel; they operate on nine AMSU-A channels above 52 GHz, the cosine of the viewing angle ϕ from nadir, and a land-sea flag (see Fig. 2). They were trained on seven orbits spaced over one year for latitudes up to $\pm 55°$. Inferred 50- and 15-km precipitation-induced perturbations at 52.8 GHz are shown in Fig. 3(c) and (d) for a frontal system. Such estimates of 15-km perturbations near 54 GHz help characterize heavily precipitating small cells.

Such inferred 15-km-resolution perturbations at 52.8, 53.6, 54.4, 54.9, and 55.5 GHz are then combined with

1) 183±1-, 183±3-, and 183±7-GHz 15-km HSB data;
2) leading three principal components characterizing the original five corrected 50-km AMSU-A temperature radiances;
3) two surface-insensitive principal components that characterize the window channels at 23.8, 31.4, 50, and 89 GHz, plus the four HSB channels.

All 13 of these variables, plus the secant of the satellite zenith angle θ, are fed into the neural net used for 15-km precipitation rate retrievals, as shown in Fig. 2. The relative insensitivity of these inputs to surface emissivity are important to the success of this technique over land, ice, and snow.

This network was trained to minimize the rms value of the difference between the logarithms of the (AMSU + 1-mm/h) and (NEXRAD + 1-mm/h) retrievals; use of logarithms reduced the emphasis on the heaviest rain rates, which were roughly three orders of magnitude greater than the lightest rates. Adding 1 mm/h reduced the emphasis on the lightest rain rates which are more noise-dominated. These intuitive choices clearly impact the retrieval error distribution, and therefore further study should enable algorithm improvements. Retrievals with training optimized for low rain rates did not markedly improve that regime, however. NEXRAD precipitation retrievals with 2-km resolution were smoothed to approximate Gaussian spatial averages that were centered on and approximated the view-angle-distorted 15- or 50-km antenna beam patterns. The accuracy of NEXRAD precipitation observations is known to vary with distance, so only points beyond 30 km but within 110 km of each NEXRAD radar site were included in the data used to train and test the neural nets. Eighty different networks were trained using the Levenberg–Marquardt algorithm, each with different numbers of nodes and water vapor principal components. A network with nearly the best performance over the testing dataset was chosen; it used two surface-blind

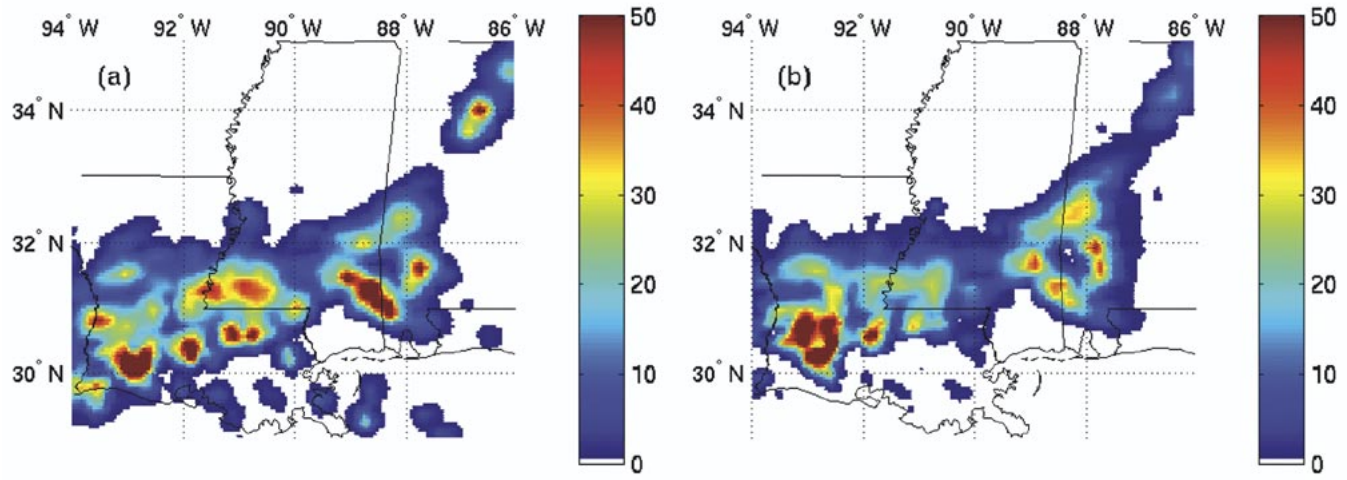

Fig. 4. Precipitation rates (millimeters per hour) above 0.5 mm/h observed September 13, 2000, 1030 UTC. (a) Fifteen-kilometer-resolution NEXRAD retrieval and (b) 15-km-resolution AMSU retrieval.

water vapor principal components, and only slightly better performance was achieved with five water vapor principal components with increased surface sensitivity. The final network had one hidden layer with five nodes that used the tanh sigmoid function. These neural networks are similar to those described in [1]. The resulting 15-km-resolution precipitation retrievals are then smoothed to yield 50-km retrievals.

The 15-km retrieval neural network was trained using precipitation data from the 38 orbits listed in Table II. During this period the radio interference to AMSU-B was negligible relative to other sources of retrieval error. Each 15-km pixel flagged as potentially precipitating using 183±7- or 183±3-GHz radiances (see Figs. 1 and 2) was used either for training, validation, or testing of the neural network. For these 38 orbits over the United States, 15 160 15-km pixels were flagged and considered suitable for training, validation, and testing; half were used for training; and one quarter were used for each of validation and testing, where the validation pixels were used to determine when the training of the neural network should cease. Based on the final AMSU and NEXRAD 15-km retrievals, approximately 14 and 38%, respectively, of the flagged 15-km pixels appear to have been precipitating less than 0.1 mm/h for the test set.

III. Retrieval Performance Evaluation

This section presents three forms of evaluation for this initial precipitation-rate retrieval algorithm: 1) representative qualitative comparisons of AMSU and NEXRAD precipitation rate images, 2) quantitative comparisons of AMSU and NEXRAD retrievals stratified by NEXRAD rain rate, and 3) representative precipitation images at more extreme latitudes beyond the NEXRAD training zone.

A. Image Comparisons of NEXRAD and AMSU/HSB Retrievals

Each NEXRAD comparison at 15-km resolution occurred within ∼8 min of satellite overpass; such coincidence is needed to characterize single-pixel retrievals because convective precipitation evolves rapidly on this spatial scale. Although comparison with instruments such as TRMM and SSM/I would be useful, their orbits unfortunately overlap those of AMSU within 8 min so infrequently (if ever) that comparisons over precipitation will be too rare to be useful until several years of data have been analyzed. This challenge of simultaneity and the sporadic character of rain have restricted most prior instrument comparisons (passive microwave satellites, radar, rain gauges) to dimensions over 100 km and to periods of an hour to a month [4]–[6]. The uniformity and extent of the NEXRAD network offer a unique degree of simultaneity on 15- and 50-km scales and even the ability to match the Gaussian shape of the AMSU antenna beams.

Although these AMSU/HSB–NEXRAD comparisons are encouraging because they involve single pixels and independent physics and facilities, further extensive analyzes are required for real validation. For example, comparisons of precipitation averages and differences over the same time/space units used to validate other precipitation measurement systems (e.g., SSM/I [9], ATOVS, TRMM, rain gauges) will be needed to characterize variances and systematic biases based on precipitation rate, type, location, or season. These biases will include any present in the NEXRAD data used to train the AMSU/HSB algorithm; once characterized, they can be diminished. Any excess variance experienced for rain cells too small to be resolved by AMSU/HSB can also eventually be better characterized, although it is believed to be modest for cells with microwave signatures larger than ∼10 km. Smaller cells contribute little to total rainfall.

Fig. 4(a) and (b) presents 15-km-resolution precipitation retrieval images for September 13, 2000 obtained from NEXRAD and AMSU, respectively. On this occasion, both sensors yield rain rates over 50 mm/h at similar locations and lower rain rates down to 0.5 mm/h over comparable areas. The revealed morphology is thus very similar even though AMSU observes ∼6 min before NEXRAD, and they sense altitudes that may be separated by several kilometers; rain falling at a nominal rate of 10 m/s takes 10 min to fall 6 km.

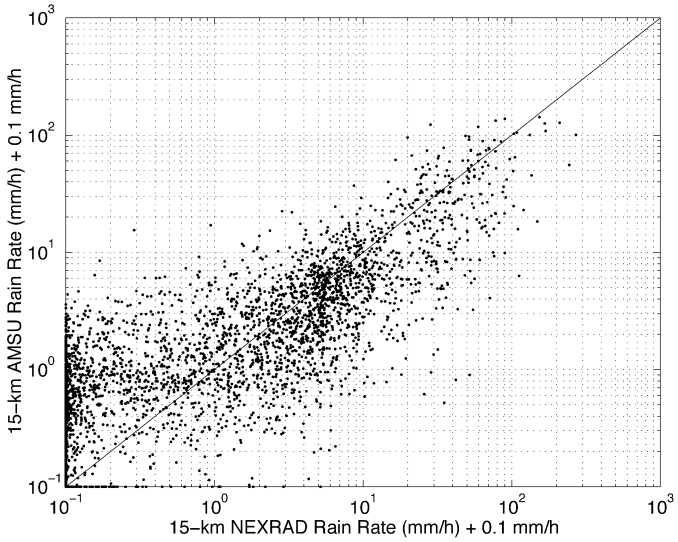

Fig. 5. Comparison of AMSU and NEXRAD estimates of rain rate at 15-km resolution.

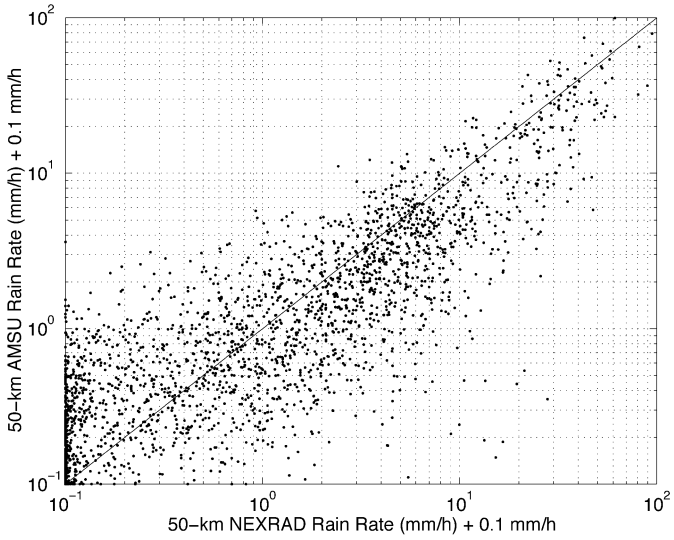

Fig. 6. Comparison of AMSU and NEXRAD estimates of rain rate at 50-km resolution.

B. Numerical Comparisons of NEXRAD and AMSU/HSB Retrievals

Fig. 5 shows the scatter between the 15-km AMSU and NEXRAD rain-rate retrievals for the test pixels not used for training or validation. Fig. 6 shows the scatter between the 50-km AMSU and NEXRAD rain-rate retrievals over all points flagged as precipitating.

The relative sensitivity of AMSU and NEXRAD to light and heavy rain can be seen from Fig. 6. In general, these figures suggest that AMSU responds less to the highest radar rain rates, perhaps because AMSU is less sensitive to the bright-band or hail anomalies that affect radar. They also suggest the risk of false rain detections increases for AMSU retrievals below $\sim$0.5 mm/h at 50-km resolution, although further study will be required. Greater accuracy at these low rates will require more space-time averaging and careful calibration. The risk of overestimating rain rate also appears to be limited. Only 3.3% of the total AMSU-derived rainfall was in areas where AMSU saw more than 1 mm/h and NEXRAD saw less than 1 mm/h. Only 7.6% of the total NEXRAD-derived rainfall was in areas where NEXRAD saw more than 1 mm/h and AMSU saw less than 1 mm/h. These percentages can be compared to the total percentages of AMSU and NEXRAD rain that fell at rates above 1 mm/h, which are 94 and 97, respectively. It is also interesting to see to what degree each sensor retrieves rain when the other does not, and how much rain each sensor misses. For example, of the 73 NEXRAD 15-km rain rate retrievals in Fig. 5 above 54 mm/h, none were found by AMSU to be below 3 mm/h, and of the 61 AMSU 15-km retrievals above 45 mm/h, none were found by NEXRAD to be below 16 mm/h. Also, of the 69 NEXRAD 50-km rain rate retrievals in Fig. 6 above 30 mm/h, none were found by AMSU to be below 5 mm/h, and of the 102 AMSU 50-km retrievals above 16 mm/h, none were found by NEXRAD to be below 10 mm/h.

Perhaps the most significant AMSU precipitation performance metric is the rms difference between the NEXRAD and AMSU rain rate retrievals; these are grouped by retrieved NEXRAD rain rates in octaves. The central 26 AMSU-A scan angles and central 78 AMSU-B scan angles were included in these evaluations; only the outermost two AMSU-A angles on each side were omitted. These comparisons used all 50-km pixels and only those 15-km pixels not used for training or validation. The results are listed in Table III. The smoothing of the 15-km NEXRAD and AMSU results to nominal 50-km resolution was consistent with an AMSU-A Gaussian beamwidth of 3.3°.

TABLE III
RMS AMSU/NEXRAD DISCREPANCIES (IN MILLIMETERS PER HOUR)

NEXRAD range	15-km resolution	50-km resolution
<0.5 mm/h	1.0	0.5
0.5-1 mm/h	2.0	0.9
1-2 mm/h	2.3	1.1
2-4 mm/h	2.7	1.8
4-8 mm/h	3.5	3.2
8-16 mm/h	6.9	6.6
16-32 mm/h	19.0	12.9
>32 mm/h	42.9	22.1

The rms agreement between these two very different precipitation-rate sensors appears surprisingly good, particularly since a single AMSU neural network is used over all angles, seasons, and latitudes. The 3-GHz radar retrievals respond most strongly to the largest hydrometeors, especially those below the bright band near the freezing level, while AMSU interacts with the general population of hydrometeors in the top few kilometers of the precipitation cell, which may lie several kilometers above the freezing level. Much of the agreement between AMSU and NEXRAD rain-rate retrievals must therefore result from the statistical consistency of the relations between rain rate and its various electromagnetic signatures. It is difficult to say how much of the observed discrepancy is due to each sensor or to say how well each correlates with precipitation reaching the ground.

This study furthermore provided an opportunity for evaluation of radar data. The rms discrepancies between AMSU and

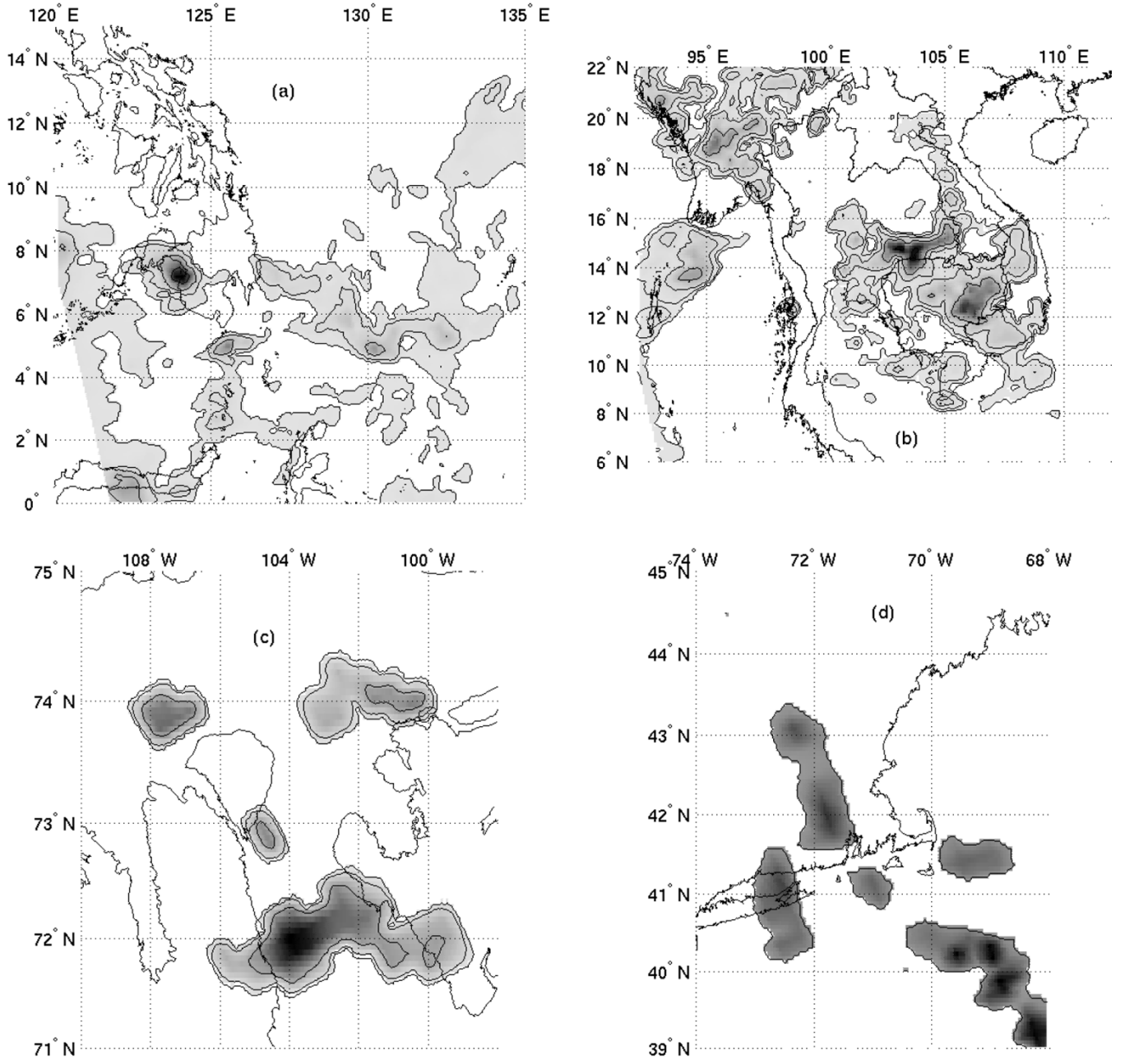

Fig. 7. AMSU precipitation rate retrievals (mm/h) with 15-km resolution. (a) Philippines, April 16, 2000, (b) Indochina, July 5, 2000, (c) Canada, August 2, 2000, and (d) New England snowstorm, March 5, 2001. Precipitation rate retrievals exceed 0.5 mm/h in the shaded regions, and contours are drawn for 0.5, 2, 8, 32, and 128 mm/h. The peak retrieved values are 47, 143, 30, and 1.5 mm/h in (a)–(d), respectively.

NEXRAD retrievals were separately calculated over all points at ranges from 110–230 km from any radar. For NEXRAD precipitation rates below 16 mm/h, these rms discrepancies were approximately 40% greater than those computed for test points at 30–110-km range. At rain rates greater than 16 mm/h, the accuracies beyond 110 km were more comparable. Most points in the eastern U.S. are more than 110 km from any NEXRAD radar site.

IV. Global Retrievals of Rain and Snow

One of the principal Aqua validation activities will involve testing and tuning of the precipitation retrievals for climates not well represented in the NEXRAD training dataset. Fig. 7 illustrates precipitation-rate retrievals at points around the globe where radar confirmation data is scarce. Fig. 7(a) shows precipitation retrievals in the tropics over a mix of land and sea, while Fig. 7(b) shows a more intense tropical event. Fig. 7(c) illustrates strong precipitation near 72° to 74 °N, again over both land and sea. Finally, Fig. 7(d) illustrates the March 5, 2001, New England snowstorm that deposited roughly a foot of snow within a few hours: an accumulation somewhat greater than is indicated by the retrieved rain rates of ∼1.2 mm/h. This applicability of the algorithm to snowfall rate should be expected because the observed radio emission originates exclusively at high altitudes. Whether the hydrometeors are rain or snow upon im-

pact depends only on air temperatures near the surface, far below those altitudes being probed. For essentially all of the pixels shown in Fig. 7, the adjacent clear air exhibited temperature and humidity profiles (inferred from AMSU) within the range of the training set. Nonetheless regional biases are expected and will require evaluation. For example, polar stratiform precipitation is expected to exhibit relatively weaker radiometric signatures in winter when the temperature lapse rates are lower, and snow-covered mountains in cold polar air can produce false detections.

V. Conclusion

These evaluations of rain rate with 15- and 50-km nominal resolution suggest that AIRS/AMSU/HSB rain rate retrievals will usefully supplement other global precipitation datasets over both land and sea at rates approaching 100 mm/h and that an early scientific objective of the Aqua program should be to reconcile and intercalibrate these various approaches. They also suggest that most 15-km spots precipitating more than 1 mm/h should be readily identifiable. It also appears likely that further training and validation would be helpful for atmospheric conditions remote from those occurring in the eastern United States.

Acknowledgment

The authors wish to thank P. W. Rosenkranz, E. Williams, and M. M. Wolfson for helpful discussions, and S. P. L. Maloney, and C. Lebell for assistance with the NEXRAD data.

References

[1] D. H. Staelin and F. W. Chen, "Precipitation observations near 54 and 183 GHz using the NOAA-15 satellite," *IEEE Trans. Geosci. Remote Sensing*, vol. 38, pp. 2322–2332, Sept. 2000.

[2] B. H. Lambrigtsen, "Calibration of the AIRS microwave instruments," *IEEE Trans. Geosci. Remote Sensing*, vol. 41, pp. 369–378, Feb. 2003.

[3] G. L. Stephens *et al.*, "The CloudSat mission and the A-train: A new dimension of space-based observations of clouds and precipitation," *Bull. Amer. Meteorol. Soc.*, vol. 83, no. 12, pp. 1771–1790, 2002.

[4] P. A. Arkin and P. Xie, "The global precipitation climatology project: First algorithm intercomparison project," *Bull. Amer. Meteorol. Soc.*, vol. 75, no. 3, pp. 401–420, 1994.

[5] E. A. Smith *et al.*, "Results of WetNet PIP-2 project," *J. Atmos. Sci.*, vol. 55, no. 9, pp. 1483–1536, May 1998.

[6] R. F. Adler *et al.*, "Intercomparison of global precipitation products: The third precipitation intercomparison project (PIP-3)," *Bull. Amer. Meteorol. Soc.*, vol. 82, no. 7, pp. 1377–1396, July 2001.

[7] W. J. Blackwell *et al.*, "NPOESS aircraft sounder testbed-microwave (NAST-M): Instrument description and initial flight results," *IEEE Trans. Geosci. Remote Sensing*, vol. 39, pp. 2444–2453, Nov. 2001.

[8] A. J. Gasiewski *et al.*, "Airborne imaging of tropospheric emission at millimeter and submillimeter wavelengths," in *Proc. IGARSS*, Aug. 1994, pp. 663–665.

[9] M. D. Conner and G. W. Petty, "Validation and intercomparison of SSM/I rain-rate retrieval methods over the continental U.S.," *J. Appl. Meteorol.*, vol. 37, no. 7, pp. 679–700, 1998.

Frederick W. Chen (S'97) received the S.B. and M.Eng. degrees in electrical engineering from the Massachusetts Institute of Technology (MIT), Cambridge, in 1998. He is currently pursuing the Ph.D. degree at MIT.

During the summer of 1996, he worked as a Summer Intern in the Reactor Analysis Division, Argonne National Laboratory, Argonne, IL, on machine condition monitoring using maximum-likelihood estimation and neural nets. Since 1997, he has been with the Remote Sensing and Estimation Group, MIT Research Laboratory of Electronics, studying methods for estimating precipitation rates from passive microwave spectrometers on meteorological satellites and aircraft.

Mr. Chen received first prize in the Student Prize Paper Competition at IGARSS 2002.

David H. Staelin (S'59–M'65–SM'75–F'79) received the B.S., M.S., and Sc.D. degrees in electrical engineering from the Massachusetts Institute of Technology (MIT), Cambridge, in 1960, 1961, and 1965, respectively.

He joined the MIT faculty in 1965, where he is currently Professor of electrical engineering and teaches electromagnetics and signal processing. He was a Principal Investigator for the NEMS and SCAMS microwave spectrometer experiments on the National Aeronautics and Space Administration's (NASA) Nimbus-5 and Nimbus-6 satellites, and a Co-Investigator for the NASA AIRS/AMSU/HSB sounding experiment on Aqua, SMMR microwave experiment on Nimbus 7, and Planetary Radio Astronomy Experiment on Voyager 1 and 2. Other research has involved radio astronomy, video coding, milliarc-second optical astrometry, and random process characterization. From 1990 to 2001, he was Assistant Director of the MIT Lincoln Laboratory.